



**HAL**  
open science

## Determination of the Intracellular Complexation of Inorganic and Methylmercury in Cyanobacterium *Synechocystis* sp. PCC 6803

Javier Garcia-Calleja, Thibaut Cossart, Zoyne Pedrero, João Santos, Laurent Ouerdane, Emmanuel Tessier, Vera Slaveykova, David Amouroux

► **To cite this version:**

Javier Garcia-Calleja, Thibaut Cossart, Zoyne Pedrero, João Santos, Laurent Ouerdane, et al.. Determination of the Intracellular Complexation of Inorganic and Methylmercury in Cyanobacterium *Synechocystis* sp. PCC 6803. *Environmental Science and Technology*, 2021, 55 (20), pp.13971-13979. 10.1021/acs.est.1c01732 . hal-03439343

**HAL Id: hal-03439343**

**<https://hal.science/hal-03439343v1>**

Submitted on 23 Nov 2021

**HAL** is a multi-disciplinary open access archive for the deposit and dissemination of scientific research documents, whether they are published or not. The documents may come from teaching and research institutions in France or abroad, or from public or private research centers.

L'archive ouverte pluridisciplinaire **HAL**, est destinée au dépôt et à la diffusion de documents scientifiques de niveau recherche, publiés ou non, émanant des établissements d'enseignement et de recherche français ou étrangers, des laboratoires publics ou privés.

1           **Determination of the intracellular complexation of inorganic and**  
2           **methylmercury in cyanobacterium *Synechocystis* sp. PCC 6803.**

3  
4   Javier Garcia-Calleja\*<sup>1</sup>, Thibaut Cossart<sup>2</sup>, Zoyne Pedrero\*<sup>1</sup>, João P. Santos<sup>2</sup>, Laurent Ouerdane<sup>1</sup>,  
5                                   Emmanuel Tessier<sup>1</sup>, Vera I. Slaveykova<sup>2</sup>, David Amouroux<sup>1</sup>

6   <sup>1</sup> Université de Pau et des Pays de l'Adour, E2S UPPA, CNRS, IPREM, Institut des Sciences  
7   Analytiques et de Physico-chimie pour l'Environnement et les matériaux, Pau, France,

8   <sup>2</sup> University of Geneva, Faculty of Sciences, Earth and Environment Sciences, Department F.-A.  
9   Forel for Environmental and Aquatic Sciences, Uni Carl Vogt, 66 Bvd. Carl Vogt, CH-1211  
10   Geneva, Switzerland

11  
12   **Corresponding Authors:**

13   Javier Garcia-Calleja E-mail: [javier.garcia-calleja@univ-pau.fr](mailto:javier.garcia-calleja@univ-pau.fr) (J.C) phone: +34 669159412

14   Zoyne Pedrero E-mail: [zoyne.pedrerorozayas@univ-pau.fr](mailto:zoyne.pedrerorozayas@univ-pau.fr) (Z.P) phone: +33 540175027

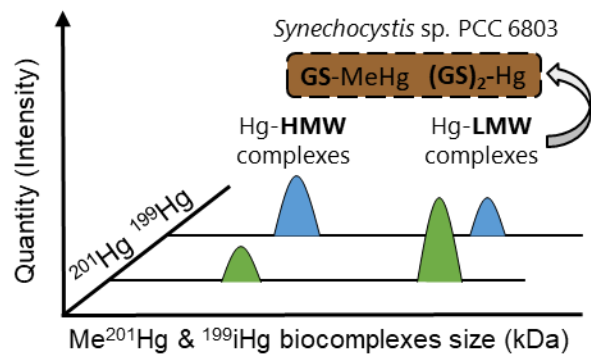
15

16 **ABSTRACT.**

17 Understanding of mercury (Hg) complexation with low molecular weight (LMW) bioligands will  
18 help elucidate its speciation. In natural waters, the rate of this complexation is governed by  
19 physicochemical, geochemical and biochemical parameters. However, the role of bioligands  
20 involved in Hg intracellular handling by aquatic microorganisms is not well documented. Here,  
21 we combine the use of isotopically-labelled Hg species (inorganic and monomethyl mercury, iHg  
22 & MeHg) with gas or liquid chromatography coupling to elemental and molecular mass  
23 spectrometry to explore the role of intracellular biogenic ligands involved in iHg and MeHg  
24 speciation in cyanobacterium *Synechocystis* sp. PCC 6803, a representative phytoplankton species.  
25 This approach allowed us to track resulting metabolic and newly-found intracellular Hg  
26 biocomplexes (e.g. organic thiols) in *Synechocystis* sp. PCC 6803 finding different intracellular  
27 Hg species binding affinities with both high and low molecular weight (HMW & LMW) bioligands  
28 in the exponential and stationary phase. Furthermore, the parallel detection with both elemental  
29 and molecular ionization sources allowed the sensitive detection and molecular identification of  
30 glutathione (GSH) as the main low molecular weight binding ligand to iHg ((GS)<sub>2</sub>-Hg) and MeHg  
31 (GS-MeHg) in the cytosolic fraction. Such novel experimental approach expands our knowledge  
32 on the role of biogenic ligands involved in iHg and MeHg intracellular handling in  
33 cyanobacterium.

34 **KEYWORDS:** Phytoplankton, cyanobacteria, Hg speciation, LMW thiols, mass spectrometry,  
35 glutathione.

36 **Graphical abstract:**



37

38

## 39 INTRODUCTION

40 Thiols are known to be important ligands for trace metals and known to affect the speciation of  
41 several trace metals, such as Ag, Cd, Hg, their bioavailability and transformations in aquatic  
42 environment. For example, thiols form complexes with inorganic mercury (iHg) and  
43 monomethylmercury (MeHg) with structures of  $\text{Hg}(\text{SR})_2$  or  $\text{MeHgSR}$  (R-S- being a thiolate  
44 organic ligand)<sup>7</sup>. Therefore, the characterization of resulting Hg-biocomplexes together with their  
45 quantification will provide an important information about the role of LMW thiol bioligands  
46 involved in Hg speciation and bioavailability. Indeed, freshwater alga *Selenastrum capricornutum*  
47 was exposed to MeHg complexed by environmental relevant thiols to study the influence of the  
48 chemical structure and thermodynamic stability of MeHg complexes<sup>8</sup>. The complexation of iHg  
49 and MeHg with bioligands, such as thiols, could also promote several abiotic and biotic  
50 transformations such as reduction, methylation or demethylation but also, the iHg and MeHg  
51 bioaccumulation<sup>10-12</sup>. The intracellular bioligands could sequester Hg compounds thus  
52 detoxifying mercury and affecting its trophic transfer<sup>13,14</sup>. Beside our improved knowledge about  
53 microbial Hg speciation in environment, the factors that control the intracellular iHg and MeHg  
54 speciation and thus toxicity outcome are poorly understood.

55 Recent advanced state-of-the-art analytical methodologies for the determination of low molecular  
56 weight (LMW) thiols in aquatic system have been developed based on a derivatization step with  
57 several reagents to enhance their chemical stability before the analysis<sup>1-5</sup>. Thiols can be separated  
58 by liquid chromatography (LC) and detected by fluorescence<sup>1</sup>, molecular absorption  
59 (ultraviolet/visible detection)<sup>6</sup> or electrospray ionization (ESI) coupled to tandem mass  
60 spectrometry (LC-ESI-MS/MS)<sup>2</sup>. For example, six LMW thiols (mercaptoacetic acid, cysteine,  
61 homocysteine, N-acetyl-cysteine, mercaptoethane-sulfonate and glutathione) with concentrations

62 from 7 to 153 nM were determined in a freshwater lake and three boreal wetlands<sup>2</sup>. Also, five  
63 LMW thiols (cysteine, thioglycolic acid, N-acetyl-L-cysteine, 3-mercaptopropionic acid and  
64 glutathione) were detected ranging from nM to  $\mu$ M levels in wetland interstitial waters<sup>1</sup>. Several  
65 LMW thiols were found in benthic biofilm and green algae's periphyton dominated by cysteine  
66 and 3-mercaptopropionic acid in the Bolivian Altiplano lakes<sup>3</sup>. Furthermore, studies focused on  
67 biofilms revealed that the extracellular thiols concentration were up to 3 orders of magnitude  
68 higher in biofilms than that in the surrounding water suggesting that microorganisms in the biofilm  
69 could have a significant impact on Hg bioavailability through the excretion of LMW thiols<sup>5</sup>. The  
70 quantification of 6 to 14 LMW thiol compounds with variable concentrations was also achieved  
71 in the extracellular medium of anaerobic bacteria, in boreal wetland porewaters and in two coastal  
72 sea waters<sup>4</sup>. Additionally, a recent novel analytical methodology was developed by optimizing  
73 online preconcentration via solid phase extraction (SPE). Achieving detection limits at pM levels  
74 and allowing the quantification of several MeHg-thiol complexes in the extracellular fraction of  
75 the bacterium *Geobacter sulfurreducens* PCA previously exposed to 100 nM of iHg<sup>9</sup>. However,  
76 the determination of Hg-biocomplexes in phytoplankton at environmental realistic concentration  
77 has not been reported yet in aquatic system and need to be fulfilled for a better understanding of  
78 the role of bioligands in Hg speciation.

79 Hyphenated techniques based on liquid chromatography coupled to inductively coupled plasma  
80 mass spectrometry (ICP-MS) and/or molecular mass spectrometry have been implemented to look  
81 into the wide spectrum at low and high molecular weight (HMW) Hg biocomplexes<sup>15</sup>. Particularly,  
82 the use of hydrophilic interaction liquid chromatography (HILIC) coupled in parallel detection  
83 with ICP-MS and ESI-MS/MS have been used to identify the structural characterization of several  
84 metal-complexes in different biological matrices. For example, the identification of Hg bound to

85 several biothiols in plants<sup>16</sup>, the characterization of Hg-metallothioneins complexes in dolphin  
86 liver<sup>17</sup> and selenium metabolites in human urine and blood<sup>18</sup> among others<sup>19</sup>. A recent study using  
87 high-resolution mass spectrometry revealed that the molecular composition of Hg binding  
88 dissolved organic matter (DOM) released by green algae *Chlorella vulgaris*, *Chlamydomonas*  
89 *reinhardtii* and *Scenedesmus obliquus* depended on natural variation in light intensity and other  
90 physicochemical parameters<sup>20</sup>.

91 Isotopically labelled Hg species were employed for the identification of iHg and MeHg binding  
92 affinities to biomolecules in living aquatic organisms<sup>21</sup>. But also, their localization in different cell  
93 compartments in methylating and non-methylating sulfate reducing bacteria was achieved<sup>15</sup>. In this  
94 previous work, the combination of Hg enriched isotopes with gas chromatography (GC)/LC-ICP-  
95 MS demonstrated that HMW bioligands released from a methylating strain were exclusively bound  
96 to MeHg, however, no structural characterization was provided. The identification of Hg binding  
97 HMW proteins requires several purification steps in order to characterize the target protein<sup>22</sup>.

98 The existing literature of Hg biocomplexes characterization in aquatic microorganisms is limited  
99 in terms of molecular mass spectrometry characterization. Using X-ray absorption spectroscopy  
100 high energy resolution fluorescence detected X ray absorption near edge structure (XAS-HERFD-  
101 XANES or HR-XANES), several Hg species were identified inside biological cells<sup>23-25</sup>. But also,  
102 X-ray absorption spectroscopy fine structure (EXAFS) can be used to elucidate the structural  
103 characterization of thiol functional groups among others (O/N) binding iHg<sup>26,27</sup>.

104 In this work, the study of intracellular complexation of Hg species was carried out by taking  
105 advantage of the tracking with isotopically enriched isotopes at low Hg concentration (3 nM / 600  
106 ng L<sup>-1</sup> <sup>199</sup>iHg & 0.3 nM / 60 ng L<sup>-1</sup> Me<sup>201</sup>Hg), one of the lowest reported so far for Hg species

107 incubation with photosynthetic unicellular organisms. The enriched isotopic tracers ( $^{199}\text{iHg}$  and  
108  $\text{Me}^{201}\text{Hg}$ ) were added after cells resuspension in the exposure medium with the purpose of tracing  
109 the newly formed Hg biocomplexes in the cytosolic fraction. The main aim of this research was to  
110 characterize Hg-biocomplexes involved in Hg speciation and to study different Hg species specific  
111 binding affinities at two different growth phases in the intracellular fraction of the cyanobacterium  
112 *Synechocystis* sp. PCC 6803. This model cyanobacterium is representative from freshwater  
113 ecosystems, a prokaryotic cell with a single chromosome free in cytoplasm and capable of growth  
114 by oxygenic photosynthesis or by glycolysis and oxidative phosphorylation in dark conditions; a  
115 phytoplankton microorganism structurally and metabolically more similar to bacteria than an  
116 eukaryotic cell that can be found in microbial and phytoplankton communities<sup>28,29</sup>. Then, the  
117 combination of complementary information obtained by hyphenated analytical techniques such as  
118 GC-ICP-MS, size exclusion chromatography (SEC) -ICP-MS and HILIC-ICP/ESI-MS provide  
119 new insights on the role of intracellular ligands in Hg speciation and intracellular fate in  
120 photosynthetic microorganisms.

121



## 122 MATERIAL AND METHODS.

123 **Reagent and Standards.** All solutions were prepared using ultrapure water (18 MΩ cm,  
124 Millipore). All samples and standards were prepared with trace metal grade acid (Fisher Scientific  
125 Illkrich, France). Working standard solutions were prepared daily by appropriate dilution of the  
126 stock standard solutions in 1% of hydrochloric acid (HCl) and stored at 4 °C until use. <sup>199</sup>Hg-  
127 enriched inorganic mercury and <sup>201</sup>Hg-enriched methylmercury (ISC-Science, Oviedo, Spain)  
128 were used as incubation spikes or tracers. <sup>198</sup>Hg-enriched inorganic mercury and <sup>202</sup>Hg-enriched  
129 methylmercury were used to quantify the endogenous Hg species (<sup>199</sup>iHg and Me<sup>201</sup>Hg) present in  
130 the bulk and cytosolic fraction. Hg species were derivatized by using sodium tetraethyl borate  
131 (NaBEt<sub>4</sub>, Merseburger spezial Chemikalien, Germany). Glutathione standard was purchased from  
132 Sigma Aldrich (Saint-Quentin-Fallavier, France). The rabbit liver metallothionein-2 isoform  
133 standard was purchased from Enzo life sciences (Villeurbanne, France). Sample flasks were  
134 cleaned using three successive baths comprising an ultrasonicator bath during 1 hour in nitric acid  
135 (HNO<sub>3</sub>) 10% (v/v) (twice) and HCl 10% (v/v) (once).

136

## 137 Experimental procedure.

138 **Culture conditions:** *Synechocystis* sp. PCC 6803 was purchased from the Pasteur Culture  
139 collection of Cyanobacteria (PCC, [https://research.pasteur.fr/en/team/collection-of-](https://research.pasteur.fr/en/team/collection-of-cyanobacteria/)  
140 [cyanobacteria/](https://research.pasteur.fr/en/team/collection-of-cyanobacteria/)) and cultivated using modified BG11 medium (sodium nitrate replaced by  
141 ammonium nitrate) with illumination values of 130 μE m<sup>-2</sup> s<sup>-1</sup> and illumination regime of 14:10 h  
142 (light : dark)<sup>30</sup>

143 **Sampling procedure:** Cells coming from two different cultures in mid-exponential and stationary  
144 growth phases were harvested by centrifugation (1300 g, 15 min, 10 °C). At the exponential phase,

145 the cyanobacterial growth is not limited having a maximal number of growing cells. Contrary, the  
146 stationary phase corresponds to a situation in which growth rate and death rate are equal. The  
147 number of new cells created is limited by the growth factor and as a result, the rate of cell growth  
148 matches the rate of cell death. Under such cellular stress conditions, it has been suggested that  
149 specific genetic responses are occurring and that the release of extracellular bioligands could be  
150 enhanced<sup>31,32</sup>.

151 Cells were resuspended in 400 mL of exposure medium (composition in Table S1) to a final cell  
152 density ( $2 \times 10^7$  cell mL<sup>-1</sup>) determined by flow cytometry (Accuri C6, BD Biosciences,  
153 Switzerland). Then, 200 mL were used as biotic control to check any possible Hg spike  
154 contamination and to measure the Hg background already found in the biological system (Figure  
155 S1), while the other 200 mL were spiked with 600 ng and 60 ng of <sup>199</sup>HgCl<sub>2</sub> and Me<sup>201</sup>HgOH per  
156 L of exposure media, respectively (3 nM <sup>199</sup>iHg & 0.3 nM Me<sup>201</sup>Hg). An aliquot of 45 mL sample  
157 was taken and centrifuged (1300 g, 15 min, 10 °C) at exposure times of 5 min and 24h. Pellets  
158 were collected and cells were fractionated to membrane fraction and cytosolic fraction as described  
159 below. Three independent cell cultures were carried out and incubated simultaneously with  
160 enriched Hg isotopes. The medium was sterile and no contamination occurred with other  
161 organisms.

162 **Cell fractionation.** Each pellet aliquot was flash frozen in liquid nitrogen to stop the metabolic  
163 activity; subsequently 1.5 mL of Milli-Q water was added to the pellet. An Ultra-Sonicator (Sonics  
164 Vibra-cell, 130 W, 20 kHz) step was used for 1 minute at 50% amplitude in order to break the  
165 cells. Allowing, through a centrifugation (10000 g, 6 min) in a centrifuge 5417R (Eppendorf), the  
166 separation of cytosolic fraction (composed by organelles, heat stable proteins (HSP) and heat  
167 denatured proteins (HDP)) and membranes with cells debris<sup>33</sup>. Cytosolic fraction samples were

168 divided in aliquots and stored at -80 °C to avoid any possible protein degradation for Hg bioligands  
169 analysis. The others were acidified with 3N HNO<sub>3</sub> and stored at 4 °C for the quantification of Hg  
170 species. The scheme of the cell fractionation procedure performed for Hg species quantification  
171 and the investigation of Hg biocomplexes is displayed in Figure S2.

## 172 **Analysis of Hg binding biomolecules by SEC/HILIC-ICP-MS and HILIC-ESI-** 173 **MS.**

174 **Instrumentation.** An Agilent 1100 liquid chromatography (Agilent, Wilmington, DE) equipped  
175 with a binary HPLC pump, an autosampler, and a diode array detector was used. Also,  
176 chromatographic separations were carried out using an Agilent 1100 capillary  $\mu$ HPLC system  
177 (Agilent, Tokyo, Japan). An Agilent inductively coupled plasma mass spectrometer (ICP-MS)  
178 7500 ce (Yokogawa Analytical Systems, Tokyo, Japan) served for Hg detection and other metals  
179 (Fe, Co, Cu and Zn among others) after liquid chromatography separation. This separation system  
180 was also coupled to a linear trap quadrupole (LTQ) Orbitrap Velos mass Spectrometer (Thermo  
181 Fisher Scientific, Bremen, Germany) in parallel by means of a heated electrospray ionization  
182 source (H ESI II).

183 **Chromatographic separation (SEC and HILIC) conditions.** Hg binding biomolecules from  
184 cytosolic fraction were separated in the Superdex<sup>TM</sup> 200 HR (10 x 300mm x 13 $\mu$ m) (Cytiva life  
185 sciences) with an operation range of 10 to 600 kDa and used for a wide screening of such  
186 biomolecules. For the analysis of LMW compounds, an aliquot from the cytosol (15 $\mu$ L) was  
187 diluted with acetonitrile (1:2 v/v) in order to precipitate high molecular weight biomolecules  
188 following this procedure<sup>18,22</sup>, with a subsequent addition of 250  $\mu$ g of natural inorganic and  
189 methylated Hg per L before the injection in a TSKgel<sup>®</sup> amide 80 column (Sigma Aldrich). The  
190 hydrophilic interaction liquid chromatography has the advantage of using a polar mobile phase,

191 being compatible with electrospray ionization and enabling the parallel detection in both analytical  
192 instruments. The operating parameters for size exclusion chromatography and hydrophilic  
193 interaction liquid chromatography coupled to ICP-MS and ESI-MS analysis are shown in Table  
194 S2.

195 To accurately determine the molecular mass range that Hg binding LWM bioligands could be  
196 found in the cytosolic fraction (under 16 kDa), a screening was carried out in a Superdex<sup>TM</sup> Peptide  
197 (Cytiva life sciences) with a separation range between 7 and 0.1 kDa; noticing a match around 0.3  
198 kDa fraction with a standard of glutathione (GSH) injected with the same chromatographic settings  
199 (Figure S3).

200 We have also examined LMW bioligands binding iHg and MeHg in the extracellular medium.  
201 However, the limitations of the experimental setup and the analytical approach did not allow us to  
202 detect any bioligand binding Hg by SEC-ICPMS in the extracellular medium even after 24 hours  
203 of Hg exposure.

#### 204 **Hg species quantification.**

205 **Instrumentation.** A Thermo Electron GC (Trace) coupled to a Thermo Electron ICP-MS (X7 X  
206 series) was used for the determination of total concentration of each Hg species.

207 **Sample preparation.** The bulk and cytosolic fraction were digested with 3N HNO<sub>3</sub> under an  
208 analytical microwave (Discover and Explorer SP-D 80 system, CEM, NC USA) and analyzed by  
209 gas chromatography coupled to inductively coupled plasma mass spectrometry (GC-ICP-MS) as  
210 detailed elsewhere<sup>34</sup>. Before starting the analytical procedure, a certain amount of both enriched  
211 spikes in <sup>198</sup>iHg and Me<sup>202</sup>Hg, previously characterized in terms of isotopic abundances and  
212 concentration, were added to the vial containing the sample. After, 5 mL of an acetic acid/acetate  
213 buffer (0.1 M, pH 3.9) were aggregated with a pH adjustment to 3.9. Subsequently, Hg species

214 (endogenous and exogenous) were ethylated using NaBrEt<sub>4</sub> (5% v/v) and extracted in isooctane  
215 by automatic shaking for 20 minutes on elliptic table. Quantification of isotopically enriched  
216 <sup>199</sup>iHg and Me<sup>201</sup>Hg was carried out by applying double-double isotope dilution analysis based on  
217 isotopic pattern deconvolution.

218 **Analytical procedure.** The measurement of the isotopic composition of Hg enriched isotopes in  
219 the samples was carried out by GC-ICP-MS. Integration of the chromatographic peaks was carried  
220 out using the commercial software Thermo Plasma Lab. The methodological detection limit for  
221 iHg and MeHg were 0.05 and 0.03 ng L<sup>-1</sup> respectively. All operating parameters for the GC-ICP-  
222 MS analysis are found in Table S3. Details of the mathematical approach for quantification of the  
223 samples by double-double isotope dilution analysis are observed in Figure S4.

224

225 **RESULTS and DISCUSSION.**

226 **Hg species concentration in the cytosolic fraction.**

227 The concentration of  $^{199}\text{iHg}$  and  $\text{Me}^{201}\text{Hg}$  in the bulk (exposure medium and cells) and cytosolic  
228 fraction of *Synechosystis* sp. PCC 6803 are presented in Table 1. Overall, similar Hg distribution  
229 was observed in exponential and stationary phase. The proportion of  $^{199}\text{iHg}$  and  $\text{Me}^{201}\text{Hg}$  in the  
230 cytosolic fraction ranged between 9-10 % and 32-36 % respectively after 24 hours of Hg exposure  
231 at both growth phases. At the beginning ( $t=5\text{min}$ ), the concentration of  $^{199}\text{iHg}$  ranged between 6-8  
232  $\text{ng L}^{-1}$  whereas, for  $\text{Me}^{201}\text{Hg}$  ranged between 13-19  $\text{ng L}^{-1}$  in the cytosolic fraction. No large  
233 distinctions were found for  $\text{Me}^{201}\text{Hg}$  after 24 hours whereas, a higher uptake of  $^{199}\text{iHg}$  was  
234 observed at both growth phases.

235

236

237

238

239

240

241

242

243

244

245

246

247

248 **Table 1.**  $^{199}\text{iHg}$  and  $\text{Me}^{201}\text{Hg}$  species proportion and concentration ( $\text{ng L}^{-1}$ ) in the bulk (exposure medium  
 249 and cells) and cytosolic fraction in the beginning (5min) and after 24h exposure of *Synechocystis* sp. PCC  
 250 6803 in exponential and stationary growth phases. Mean  $\pm$  sd (n=3).

251

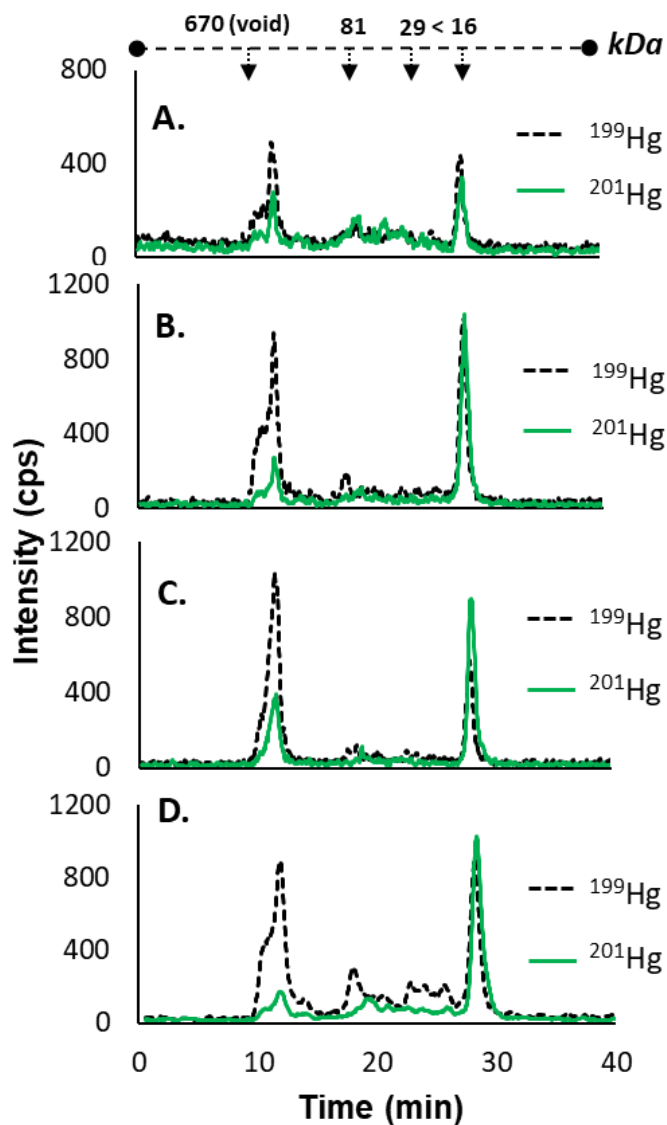
252

<i>Exponential</i> <i>phase</i>	$^{199}\text{iHg}$		$\text{Me}^{201}\text{Hg}$	
	$t_{5\text{min}}$	$t_{24\text{h}}$	$t_{5\text{min}}$	$t_{24\text{h}}$
<b>Bulk (<math>\text{ng L}^{-1}</math>)</b>	517 $\pm$ 14	379 $\pm$ 24	52 $\pm$ 1	47 $\pm$ 3
<b>Cytosolic fraction (<math>\text{ng L}^{-1}</math>)</b>	6 $\pm$ 1	35 $\pm$ 9	13 $\pm$ 1	15 $\pm$ 2
<b>Cytosolic fraction vs Bulk (%)</b>	1.2 $\pm$ 0.2	9.2 $\pm$ 2.4	25 $\pm$ 2	32 $\pm$ 4

<i>Stationary</i> <i>phase</i>	$^{199}\text{iHg}$		$\text{Me}^{201}\text{Hg}$	
	$t_{5\text{min}}$	$t_{24\text{h}}$	$t_{5\text{min}}$	$t_{24\text{h}}$
<b>Bulk (<math>\text{ng L}^{-1}</math>)</b>	549 $\pm$ 28	421 $\pm$ 23	54 $\pm$ 1	50 $\pm$ 1
<b>Cytosolic fraction (<math>\text{ng L}^{-1}</math>)</b>	8 $\pm$ 3	41 $\pm$ 7	19 $\pm$ 1	18 $\pm$ 1
<b>Cytosolic fraction vs Bulk (%)</b>	1.5 $\pm$ 0.5	9.7 $\pm$ 1.7	35 $\pm$ 2	36 $\pm$ 2

253 Hg binding bioligands screening in the cytosolic fraction.

254



255

256 **Figure 1.** Size exclusion chromatograms (Superdex 200 (Range: 600 - 10 kDa)) in the cytosolic fraction of

257 *Synechocystis* sp. PCC 6803 by ICP-MS detection of (A)  $^{199}\text{Hg}$  and  $^{201}\text{Hg}$  corresponding to both Hg isotopic

258 tracers ( $^{199}\text{iHg}$  and  $\text{Me}^{201}\text{Hg}$ ) after 5 minutes of exposure in the exponential phase. (B)  $^{199}\text{Hg}$  and  $^{201}\text{Hg}$

259 corresponding to both isotopic tracers ( $^{199}\text{iHg}$  and  $\text{Me}^{201}\text{Hg}$ ) after 24 hours of exposure in the exponential

260 phase. (C)  $^{199}\text{Hg}$  and  $^{201}\text{Hg}$  corresponding to both Hg isotopic tracers ( $^{199}\text{iHg}$  and  $\text{Me}^{201}\text{Hg}$ ) after 5 minutes



261 of exposure in the stationary phase. (D)  $^{199}\text{Hg}$  and  $^{201}\text{Hg}$  corresponding to both isotopic tracers ( $^{199}\text{iHg}$  and  
 262  $\text{Me}^{201}\text{Hg}$ ) after 24 hours of exposure in the stationary phase.

263  
 264 The analysis by SEC-ICP-MS of the cytosolic fraction reveals two main Hg-containing fractions  
 265 with HMW ( $\geq 600$  kDa, 10-13 min) and LMW ( $\leq 16$  kDa, 27-29 min) in a range from 600 to 10  
 266 kDa (Figure 1). The increase of  $^{199}\text{Hg}$  signal was correlated with the exposure time from 5 min to  
 267 24h.  $^{199}\text{iHg}$  was preferentially bound to HMW biomolecules eluting around 10-13 min at the  
 268 beginning of the Hg exposure. After 24 hours, the intensity of  $^{199}\text{iHg}$  binding HMW fraction ( $\geq 600$   
 269 kDa) remained constant whereas, a remarkable increase in  $^{199}\text{Hg}$  intensity was seen at longer  
 270 elution time corresponding to fractions of lower molecular weight; from 29 to 81 kDa (17-26 min)  
 271 and under 16 kDa (27-29 min). On the other hand,  $\text{Me}^{201}\text{Hg}$  was mostly bound to LMW fraction  
 272 exhibiting an intensity increase after 24h exposure at both growth phases.

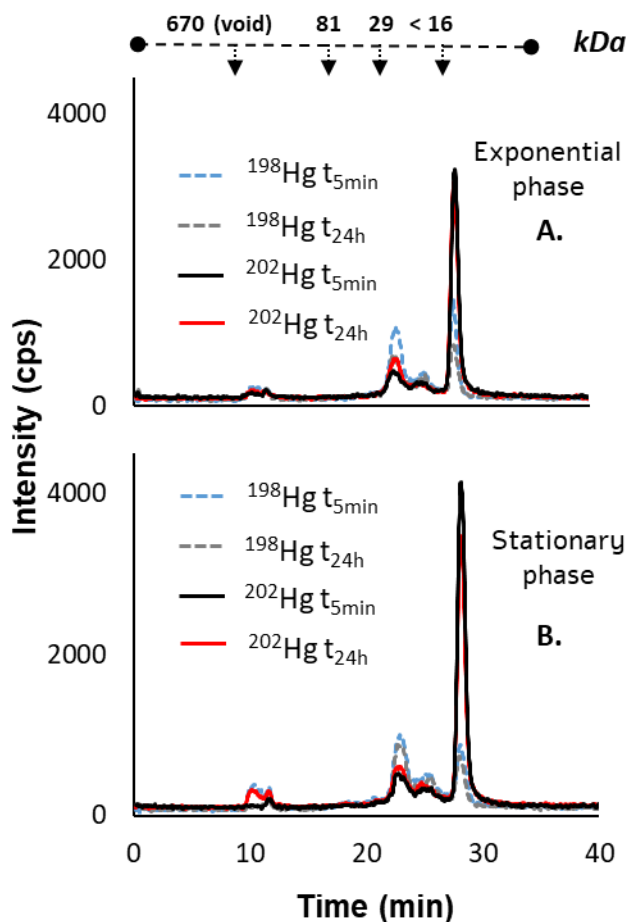
273 Despite SEC-ICP-MS analysis does not give quantitative information, we have estimated the  
 274 proportion of  $^{199}\text{iHg}$  and  $\text{Me}^{201}\text{Hg}$  bound to LMW cytosolic ligands (Table 2) based on the peak  
 275 area of eluted compounds (Figure 1).

276 **Table 2.** Percentage of  $^{199}\text{iHg}$  and  $\text{Me}^{201}\text{Hg}$  bound to LMW fraction of cytosolic ligands at the beginning  
 277 and after 24h exposure at different growth phases in *Synechocystis* sp. PCC 6803. Mean  $\pm$  sd (n=3).

% Hg binding LMW fraction	$^{199}\text{iHg}$		$\text{Me}^{201}\text{Hg}$	
	$t_{5\text{min}}$	$t_{24\text{h}}$	$t_{5\text{min}}$	$t_{24\text{h}}$
Exponential phase	38 $\pm$ 8 %	47 $\pm$ 11 %	68 $\pm$ 5%	79 $\pm$ 4%
Stationary phase	35 $\pm$ 14 %	46 $\pm$ 8 %	67 $\pm$ 4%	86 $\pm$ 9 %

278  
 279 Table 2 shows the percentage of Hg bound to the LMW fraction at the beginning and after 24  
 280 hours of Hg exposure at different growth phases in which the proportion of  $^{199}\text{iHg}$  and  $\text{Me}^{201}\text{Hg}$

281 bound to the LMW fraction after 24 hours of Hg exposure were 46-47 % and 79-86 % respectively,  
282 at both growth phases.  
283 To obtain further information about the specificity and affinity of Hg to bioligands, two different  
284 enriched Hg species ( $^{198}\text{iHg}$  and  $\text{Me}^{202}\text{Hg}$ ) were subsequently added to the cytosolic fraction that  
285 had been previously exposed to  $^{199}\text{iHg}$  and  $\text{Me}^{201}\text{Hg}$  (Figure 2).



286  
287 **Figure 2.** Size exclusion chromatograms (Superdex 200 (Range: 600-10 KDa)) in the cytosolic fraction of  
288 *Synechocystis* sp. PCC 6803 in the exponential (A) and stationary growth phase (B) by ICP-MS detection  
289 of  $^{198}\text{Hg}$  and  $^{202}\text{Hg}$  corresponding to the addition ( $5 \mu\text{g L}^{-1}$ ) of  $^{198}\text{iHg}$  and  $\text{Me}^{202}\text{Hg}$  after 5 minutes and 24  
290 hours of Hg exposure of both isotopic tracers ( $^{199}\text{iHg}$  and  $\text{Me}^{201}\text{Hg}$ ).  
291

292 The obtained results in figure 2 evidenced similar patterns to endogenous Hg biocomplexes  
293 distribution from figure 1 confirming the specific affinity of LMW fraction (27-29 min) for MeHg.  
294 But also, it demonstrates that bioligands functional groups in the LMW fraction are still available  
295 to bind iHg and MeHg.

296 Overall, the transition from exponential to stationary growth phase involves several adaptations  
297 such as changes in proteins expression involved in cell growth, protein biosynthesis involved in  
298 nutrient uptake and proteins related to energy metabolism<sup>32,35</sup>. Nutrient availability is the main  
299 critical factor that determines the growth phase changes. In the existing literature, no studies have  
300 ever reported comparisons in the distribution of iHg or MeHg binding intracellular ligands between  
301 exponential and stationary phase in phytoplankton. Under our experimental conditions, the  
302 differences in Hg exposure time or growth phase have not affected the distribution of potential  
303 bioligands capable of binding exogenous Hg. This result is important to highlight since the amount  
304 of the extracellular ligands released at the stationary phase could be higher<sup>31</sup> and was expected to  
305 influence the amount of the bioaccumulated iHg or MeHg.

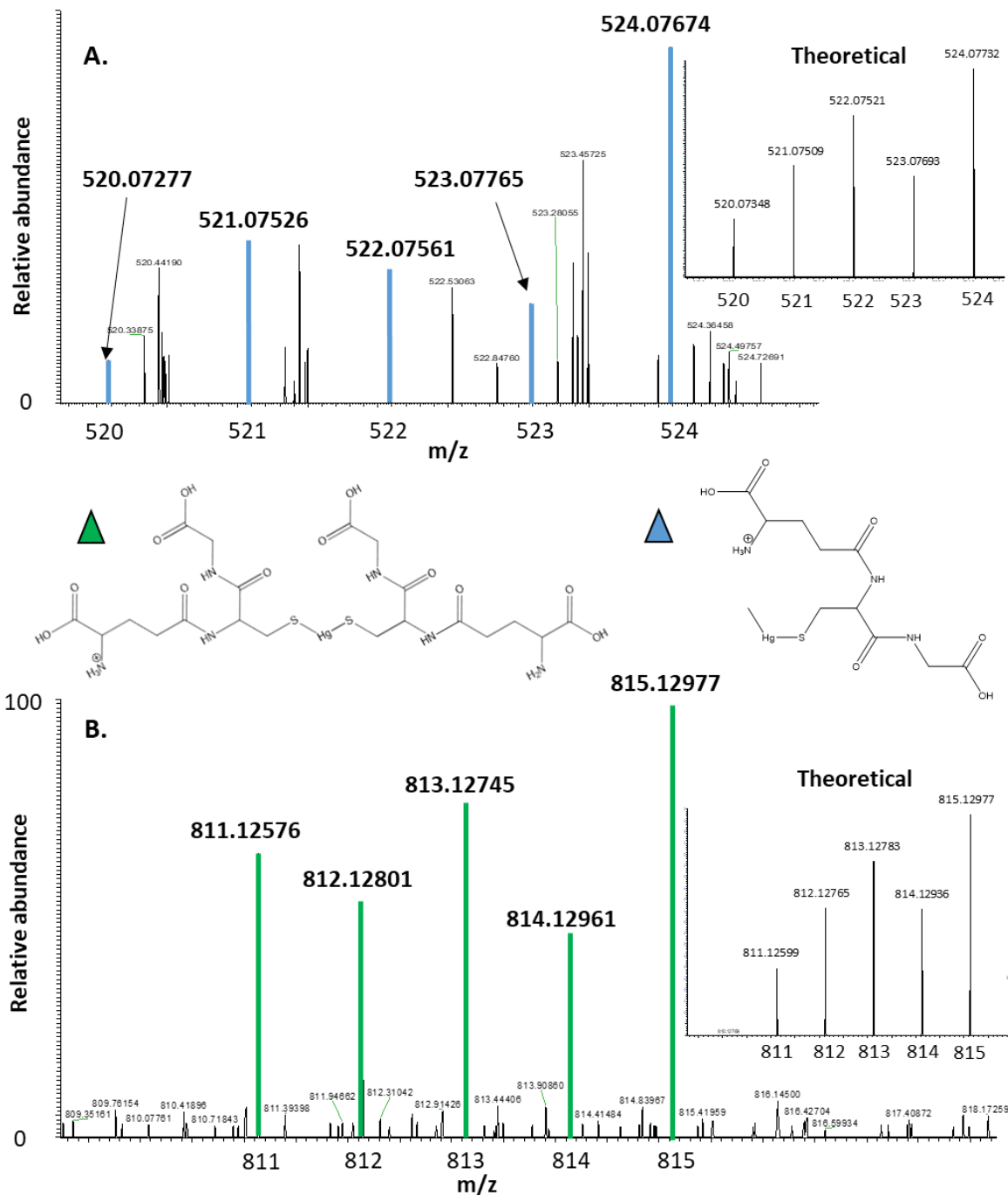
306 Understanding of iHg and MeHg intracellular fate is a key factor to explain the role of the  
307 intracellular bioligands in Hg speciation. In our work, the increase of the signal intensity of <sup>199</sup>iHg  
308 and Me<sup>201</sup>Hg bound to the LMW fraction (< 16 kDa) after 24 h in the stationary phase suggests  
309 that these specific biomolecules, where heat stable proteins among others are present, could be  
310 involved in Hg species specific sequestration at nontoxic levels. This falls in agreement with recent  
311 observations of the synthesis of glutathione and PCs by a marine diatom *Thalassiosira weissflogii*  
312 when exposed to iHg and MeHg<sup>36,37</sup>. Furthermore, the findings concerning the species specific  
313 affinity of iHg binding HMW fraction and MeHg binding LMW fraction agree with a previous  
314 study carried out with three marine phytoplankton (*Thalassiosira pseudonana*, *Chlorella*

315 *autotrophica* and *Isochrysis galbana*), where heat stable proteins were mainly binding MeHg  
316 whereas iHg was associated to the organelles fraction<sup>38</sup>. However, these experiments are not  
317 directly comparable since higher Hg concentrations were added in comparison with our work (>  
318 150 folds for iHg).

319 Although the specific function of these biogenic intracellular ligands cannot be clarified with the  
320 available data, the Hg binding bioligands detected may also be involved in several Hg  
321 transformations such as biotic reduction or biotic demethylation<sup>39,40</sup>. It should be noticed that so  
322 far only two studies reported the use of simultaneous enriched isotopes for iHg and MeHg in cell  
323 culture experiments. On one hand, to investigate the Hg species accumulation and biotic  
324 transformations in *C. reinhardtii*<sup>39</sup> and on the other hand, to explore the Hg biocomplexes  
325 distribution size in the extracellular and intracellular fraction in methylating and non methylating  
326 sulfate-reducing bacteria<sup>15</sup>. Nevertheless, no structural characterization of Hg biocomplexes was  
327 provided. Additionally, most of the studies focused on the intracellular compartment of  
328 phytoplankton cell cultures have been carried out under high Hg exposure concentrations (1000-  
329 10000 higher than our conditions), in order to study the Hg accumulation, subcellular distribution  
330 and detoxification mechanisms<sup>38-42</sup>. On the contrary, our work used lower Hg concentrations of 3  
331 nM / 600 ng L<sup>-1</sup> for <sup>199</sup>iHg and 0.3 nM / 60 ng L<sup>-1</sup> for Me<sup>201</sup>Hg. Therefore, it is not expected to  
332 have induced considerable physiological changes in the main intracellular processes<sup>43,44</sup>.  
333 Additionally, other essential elements (Cu, Zn, Fe and Co) were monitored by SEC-ICP-MS. In  
334 this case, cells that were exposed to Hg did not induce the formation of new metal-biocomplexes  
335 fractions in their SEC chromatogram profiles (Figure S5) comparing with the biotic controls (no  
336 Hg exposure).

337 **Identification of intracellular Hg species-specific biogenic complexes in the low molecular**  
338 **weight fraction.**

339 The identification of biomolecules is usually based on the retention time matching of standards  
340 and samples. However, the structural characterization provides an unambiguous identification of  
341 the molecular structure, representing a step further in terms of Hg biocomplexes determination.



342  
 343 **Figure 3. (A)** Zoom of the mass spectra obtained at 21.2 min demonstrates the presence of MeHg binding  
 344 one glutathione with its natural Hg isotopic pattern ( $^{202}\text{Hg}$   $m/z$  = 524.08). **(B).** Zoom of the mass spectra  
 345 obtained at 23.5 min demonstrate the presence of Hg binding two glutathione with its natural Hg isotopic  
 346 pattern in stationary phase ( $^{202}\text{Hg}$   $m/z$  = 815.13).

347 The analysis by HILIC-ICP-MS of the cytosolic fraction reveals two Hg binding bioligands  
348 corresponding to two different peaks with specific retention times at 21.0 min and 23.7 min (Figure  
349 S6A) based on Hg isotopes monitoring (elemental ionization). For this purpose, the injection of  
350 the same cytosolic fraction carrying out the same chromatographic settings (leading to matching  
351 retention times) was done by coupling to an electrospray ionization mass spectrometer and  
352 providing structural information about the compounds previously detected (Figure S6B). Firstly,  
353 the natural isotopic pattern of Hg was investigated in the full scan spectra at both retention times.  
354 Electrospray MS at the retention time of first peak revealed one ion with the isotopic pattern of  
355 mercury (Figure 3A) at  $m/z = 524.08$  ( $m/z$  corresponding to the most abundant isotope in the  
356 isotopic distribution). This mass to charge ratio corresponded to Hg methylated binding one  
357 glutathione (GS-MeHg,  $C_{11}H_{20}HgN_3O_6S^+$ ). Regarding the second peak, the Hg isotopic pattern  
358 was observed (Figure 3B) at  $m/z = 815.13$  corresponding to iHg binding two glutathione ((GS)<sub>2</sub>-  
359 Hg),  $C_{20}H_{33}HgN_6O_{12}S_2^+$ ). Even if the theoretical natural isotopic pattern for iHg and MeHg binding  
360 glutathione did not match in all isotopes in comparison with the experimental Hg isotopic patterns,  
361 caused by the low concentration of iHg and MeHg bound to GSH, the experimental masses agreed  
362 with the theoretical ones.

363 The present results confirmed that GSH is playing a key role in Hg sequestration in different  
364 aquatic microorganisms<sup>37,45</sup>. Particularly in cyanobacteria, GSH plays a central role in redox  
365 control of protein thiols and disulfide bonds, including protection against toxic metabolites,  
366 xenobiotic and oxidative stress<sup>46,47</sup>. Hg exposure is well known to induce accumulation of reactive  
367 oxygen species and peroxidation products in phytoplankton<sup>43</sup>. Under oxidative stress, glutathione  
368 acts as a protein reductant against highly reactive oxidants such as singlet oxygen, superoxide and  
369 hydroxyl radicals forming GS-SG<sup>29</sup>. Nevertheless, the reduction of GS-SG (S-S) to two GSH is

370 mediated by the enzyme glutathione reductase being a critical process for its regeneration.  
371 Exposure of green alga *Chlamydomonas reinhardtii* to sub-toxic concentrations of iHg and MeHg  
372 resulted in a significant increase of reduced glutathione after Hg-treatments<sup>44</sup>. GSH is a precursor  
373 of phytochelatins synthesis, which can be activated following the exposure to different toxic metals  
374 including Hg<sup>44</sup>. The cyanobacterial phytochelatin synthesis was shown to be close functionally to  
375 that of plants. Additionally, the phytochelatin synthase exhibited transpeptidasic activity during  
376 Cd- exposure, being able to synthesize phytochelatins with a degree of oligomerization higher than  
377 PC<sub>2</sub><sup>48</sup>. Furthermore, Hg exposure induced changes in intracellular thiols concentration such as  
378 glutathione or phytochelatins demonstrating that algae can control the intracellular Hg  
379 speciation<sup>36,37,40</sup>. Phytoplankton intracellular detoxification mechanisms can promote the  
380 transformation of iHg into gaseous Hg<sup>37,49</sup>. In bacteria, it was shown that the intracellular  
381 reduction is carried out enzymatically<sup>50</sup>.

382 In the extracellular fraction, several studies have demonstrated the influence of LMW bioligands  
383 on Hg speciation<sup>51,52</sup>. Particularly, high rates of iHg uptake and biotic methylation were observed  
384 in the presence of some complexing LMW thiols such as cysteine whereas, GSH inhibited these  
385 processes<sup>52</sup>. These results suggest that the molecular structure of the bioligands plays a crucial role  
386 in Hg speciation in anaerobic environments. Additional information was obtained in a freshwater  
387 green microalga *Selenastrum capricornutum*<sup>8</sup>. Skrobonja et al. 2019 showed that the  
388 thermodynamic stability in turns with the chemical structure of MeHg LMW complexes in the  
389 extracellular medium govern the rate of MeHg interactions with the cell surface<sup>8</sup>. Further  
390 investigations must be carried out to explore the role of these intra- and extra-cellular ligands in  
391 Hg speciation but also, structural studies based on molecular mass spectrometry will be needed to  
392 elucidate the exact function of the biomolecules involved in Hg speciation.



393 **Environmental perspective.**

394 The identification of glutathione as a bioligand binding to iHg ((GS)<sub>2</sub>-Hg) and MeHg (GS-MeHg)  
395 in cyanobacterium *Synechocystis* sp. PCC 6803 has demonstrated that glutathione plays an  
396 important role in Hg intracellular handling; reducing probably the potential damage that both Hg  
397 species could cause on the cellular metabolism. In aquatic environment, cyanobacteria are found  
398 in various environmental settings interacting with different aquatic microorganisms with a specific  
399 role into the natural Hg cycle. The pioneering approach based on the combination of enriched  
400 isotopes and mass spectrometry techniques represent a first step, towards explaining and  
401 understanding the intracellular speciation of iHg and MeHg in photosynthetic microorganisms.  
402 Important emphasis should be placed concerning to global warming and/or water pollution<sup>53</sup>.  
403 Particularly, cyanobacteria are considered to prevail in warmer freshwaters and their proportion  
404 will increase in phytoplankton communities<sup>54</sup>. Cyanobacteria are more resistant to pollutant  
405 exposure, high temperatures and eutrophication events caused by the global warming or nutrient  
406 contamination than other phytoplankton species<sup>55,56</sup>. Furthermore, phytoplankton communities are  
407 the main entry point in the trophic transfer for Hg. For these reasons, our results exemplify the  
408 potential bioaccumulation of iHg and MeHg at non toxic levels by a model phytoplankton.

409

410 **Notes**

411 **The authors declare no competing financial interest.**

412 **ACKNOWLEDGMENTS**

413 Financial support from Agence National de la Recherche (ARN) (Project-ANR-17-CE34-0014)  
414 and Swiss National Science Foundation (SNF) (project N 175721) in the framework of the  
415 PHYTAMBA project (PRCI ANR/SNSF). Financial support from E2S/UPPA (Energy and

416 Environment Solutions) in the framework of the MESMIC Hub (Metals in Environmental System  
417 Microbiology).

418

## 419 REFERENCES

- 420 (1) Zhang, J.; Wang, F.; House, J. D.; Page, B. Thiols in Wetland Interstitial Waters and Their  
421 Role in Mercury and Methylmercury Speciation. *Limnology and Oceanography* **2004**, *49*  
422 (6), 2276–2286. <https://doi.org/10.4319/lo.2004.49.6.2276>.
- 423 (2) Liem-Nguyen, V.; Bouchet, S.; Björn, E. Determination of Sub-Nanomolar Levels of Low  
424 Molecular Mass Thiols in Natural Waters by Liquid Chromatography Tandem Mass  
425 Spectrometry after Derivatization with p-(Hydroxymercuri) Benzoate and Online  
426 Preconcentration. *Anal. Chem.* **2015**, *87* (2), 1089–1096.  
427 <https://doi.org/10.1021/ac503679y>.
- 428 (3) Bouchet, S.; Goñi-Urriza, M.; Monperrus, M.; Guyoneaud, R.; Fernandez, P.; Heredia, C.;  
429 Tessier, E.; Gassie, C.; Point, D.; Guédron, S.; Achá, D.; Amouroux, D. Linking Microbial  
430 Activities and Low-Molecular-Weight Thiols to Hg Methylation in Biofilms and Periphyton  
431 from High-Altitude Tropical Lakes in the Bolivian Altiplano. *Environmental Science &*  
432 *Technology* **2018**, *52* (17), 9758–9767. <https://doi.org/10.1021/acs.est.8b01885>.
- 433 (4) Liem-Nguyen, V.; Huynh, K.; Gallampois, C.; Björn, E. Determination of Picomolar  
434 Concentrations of Thiol Compounds in Natural Waters and Biological Samples by Tandem  
435 Mass Spectrometry with Online Preconcentration and Isotope-Labeling Derivatization.  
436 *Analytica Chimica Acta* **2019**, *1067*, 71–78. <https://doi.org/10.1016/j.jaca.2019.03.035>.
- 437 (5) Leclerc, M.; Planas, D.; Amyot, M. Relationship between Extracellular Low-Molecular-  
438 Weight Thiols and Mercury Species in Natural Lake Periphytic Biofilms. *Environmental*  
439 *Science & Technology* **2015**, *49* (13), 7709–7716. <https://doi.org/10.1021/es505952x>.
- 440 (6) Kuśmierk, K.; Chwatko, G.; Głowacki, R.; Kubalczyk, P.; Bald, E. Ultraviolet  
441 Derivatization of Low-Molecular-Mass Thiols for High Performance Liquid  
442 Chromatography and Capillary Electrophoresis Analysis. *Journal of Chromatography B*  
443 **2011**, *879* (17–18), 1290–1307. <https://doi.org/10.1016/j.jchromb.2010.10.035>.
- 444 (7) G. Berthon. The Stability Constants of Metal Complexes of Amino Acids with Polar Side  
445 Chains. *Pure & Appl. Chem.* **1995**, *69*, 1117–1240.  
446 <https://doi.org/10.1351/PAC199567071117>.
- 447 (8) Skrobonja, A.; Gojkovic, Z.; Soerensen, A. L.; Westlund, P.-O.; Funk, C.; Björn, E. Uptake  
448 Kinetics of Methylmercury in a Freshwater Alga Exposed to Methylmercury Complexes  
449 with Environmentally Relevant Thiols. *Environ. Sci. Technol.* **2019**, *acs.est.9b05164*.  
450 <https://doi.org/10.1021/acs.est.9b05164>.
- 451 (9) Liem-Nguyen, V.; Nguyen-Ngoc, H.-T.; Adediran, G. A.; Björn, E. Determination of  
452 Picomolar Levels of Methylmercury Complexes with Low Molecular Mass Thiols by  
453 Liquid Chromatography Tandem Mass Spectrometry and Online Preconcentration. *Anal*  
454 *Bioanal Chem* **2020**. <https://doi.org/10.1007/s00216-020-02389-y>.
- 455 (10) Monperrus, M.; Tessier, E.; Amouroux, D.; Leynaert, A.; Huonnic, P.; Donard, O. F. X.  
456 Mercury Methylation, Demethylation and Reduction Rates in Coastal and Marine Surface

- 457 Waters of the Mediterranean Sea. *Marine Chemistry* **2007**, *107* (1), 49–63.  
458 <https://doi.org/10.1016/j.marchem.2007.01.018>.
- 459 (11) Lalonde, J. D.; Amyot, M.; Kraepiel, A. M. L.; Morel, F. M. M. Photooxidation of Hg(0) in  
460 Artificial and Natural Waters. *Environmental Science & Technology* **2001**, *35* (7), 1367–  
461 1372. <https://doi.org/10.1021/es001408z>.
- 462 (12) Celso, V.; Lean, D. R. S.; Scott, S. L. Abiotic Methylation of Mercury in the Aquatic  
463 Environment. *Science of The Total Environment* **2006**, *368* (1), 126–137.  
464 <https://doi.org/10.1016/j.scitotenv.2005.09.043>.
- 465 (13) Grégoire, D. S.; Poulain, A. J. A Little Bit of Light Goes a Long Way: The Role of  
466 Phototrophs on Mercury Cycling. *Metallomics* **2014**, *6* (3), 396.  
467 <https://doi.org/10.1039/c3mt00312d>.
- 468 (14) Le Faucheur, S.; Campbell, P. G. C.; Fortin, C.; Slaveykova, V. I. Interactions between  
469 Mercury and Phytoplankton: Speciation, Bioavailability, and Internal Handling: Mercury-  
470 Phytoplankton Interactions. *Environmental Toxicology and Chemistry* **2014**, *33* (6), 1211–  
471 1224. <https://doi.org/10.1002/etc.2424>.
- 472 (15) Pedrero, Z.; Bridou, R.; Mounicou, S.; Guyoneaud, R.; Monperrus, M.; Amouroux, D.  
473 Transformation, Localization, and Biomolecular Binding of Hg Species at Subcellular Level  
474 in Methylating and Nonmethylating Sulfate-Reducing Bacteria. *Environmental Science &*  
475 *Technology* **2012**, *46* (21), 11744–11751. <https://doi.org/10.1021/es302412q>.
- 476 (16) Krupp, E. M.; Milne, B. F.; Mestrot, A.; Meharg, A. A.; Feldmann, J. Investigation into  
477 Mercury Bound to Biothiols: Structural Identification Using ESI–Ion-Trap MS and  
478 Introduction of a Method for Their HPLC Separation with Simultaneous Detection by ICP-  
479 MS and ESI-MS. *Anal Bioanal Chem* **2008**, *390* (7), 1753–1764.  
480 <https://doi.org/10.1007/s00216-008-1927-x>.
- 481 (17) Pedrero, Z.; Ouerdane, L.; Mounicou, S.; Lobinski, R.; Monperrus, M.; Amouroux, D.  
482 Identification of Mercury and Other Metals Complexes with Metallothioneins in Dolphin  
483 Liver by Hydrophilic Interaction Liquid Chromatography with the Parallel Detection by ICP  
484 MS and Electrospray Hybrid Linear/Orbital Trap MS/MS. *Metallomics* **2012**, *4* (5), 473.  
485 <https://doi.org/10.1039/c2mt00006g>.
- 486 (18) Klein, M.; Ouerdane, L.; Bueno, M.; Pannier, F. Identification in Human Urine and Blood  
487 of a Novel Selenium Metabolite, Se-Methylselenoneine, a Potential Biomarker of  
488 Metabolization in Mammals of the Naturally Occurring Selenoneine, by HPLC Coupled to  
489 Electrospray Hybrid Linear Ion Trap-Orbital Ion Trap MS. *Metallomics* **2011**, *3* (5), 513.  
490 <https://doi.org/10.1039/c0mt00060d>.
- 491 (19) Trümpler, S.; Lohmann, W.; Meermann, B.; Buscher, W.; Sperling, M.; Karst, U.  
492 Interaction of Thimerosal with Proteins—Ethylmercuryadduct Formation of Human Serum  
493 Albumin and  $\beta$ -Lactoglobulin A. *Metallomics* **2009**, *1* (1), 87–91.  
494 <https://doi.org/10.1039/B815978E>.
- 495 (20) Mangal, V.; Phung, T.; Nguyen, T. Q.; Guéguen, C. Molecular Characterization of Mercury  
496 Binding Ligands Released by Freshwater Algae Grown at Three Photoperiods. *Front.*  
497 *Environ. Sci.* **2019**, *6*. <https://doi.org/10.3389/fenvs.2018.00155>.
- 498 (21) Pedrero, Z.; Mounicou, S.; Monperrus, M.; Amouroux, D. Investigation of Hg Species  
499 Binding Biomolecules in Dolphin Liver Combining GC and LC-ICP-MS with Isotopic  
500 Tracers. *J. Anal. At. Spectrom.* **2011**, *26* (1), 187–194. <https://doi.org/10.1039/C0JA00154F>.
- 501 (22) Pedrero Zayas, Z.; Ouerdane, L.; Mounicou, S.; Lobinski, R.; Monperrus, M.; Amouroux,  
502 D. Hemoglobin as a Major Binding Protein for Methylmercury in White-Sided Dolphin

- 503 Liver. *Anal Bioanal Chem* **2014**, *406* (4), 1121–1129. [https://doi.org/10.1007/s00216-013-](https://doi.org/10.1007/s00216-013-7274-6)  
504 7274-6.
- 505 (23) Manceau, A.; Nagy, K. L.; Glatzel, P.; Bourdineaud, J.-P. Acute Toxicity of Divalent  
506 Mercury to Bacteria Explained by the Formation of Dicysteinate and Tetracysteinate  
507 Complexes Bound to Proteins in *Escherichia Coli* and *Bacillus Subtilis*. *Environ. Sci.*  
508 *Technol.* **2021**, *55* (6), 3612–3623. <https://doi.org/10.1021/acs.est.0c05202>.
- 509 (24) Manceau, A.; Azemard, S.; Hédouin, L.; Vassileva, E.; Lecchini, D.; Fauvelot, C.;  
510 Swarzenski, P. W.; Glatzel, P.; Bustamante, P.; Metian, M. Chemical Forms of Mercury in  
511 Blue Marlin Billfish: Implications for Human Exposure. *Environ. Sci. Technol. Lett.* **2021**,  
512 *8* (5), 405–411. <https://doi.org/10.1021/acs.estlett.1c00217>.
- 513 (25) Manceau, A.; Gaillot, A.-C.; Glatzel, P.; Cherel, Y.; Bustamante, P. In Vivo Formation of  
514 HgSe Nanoparticles and Hg–Tetrarselenolate Complex from Methylmercury in Seabirds—  
515 Implications for the Hg–Se Antagonism. *Environ. Sci. Technol.* **2021**, *55* (3), 1515–1526.  
516 <https://doi.org/10.1021/acs.est.0c06269>.
- 517 (26) Song, Y.; Adediran, G. A.; Jiang, T.; Hayama, S.; Björn, E.; Skyllberg, U. Toward an  
518 Internally Consistent Model for Hg(II) Chemical Speciation Calculations in Bacterium–  
519 Natural Organic Matter–Low Molecular Mass Thiol Systems. *Environ. Sci. Technol.* **2020**,  
520 *54* (13), 8094–8103. <https://doi.org/10.1021/acs.est.0c01751>.
- 521 (27) Song, Y.; Jiang, T.; Liem-Nguyen, V.; Sparrman, T.; Björn, E.; Skyllberg, U.  
522 Thermodynamics of Hg(II) Bonding to Thiol Groups in Suwannee River Natural Organic  
523 Matter Resolved by Competitive Ligand Exchange, Hg L<sub>III</sub>-Edge EXAFS and <sup>1</sup>H NMR  
524 Spectroscopy. *Environ. Sci. Technol.* **2018**, *52* (15), 8292–8301.  
525 <https://doi.org/10.1021/acs.est.8b00919>.
- 526 (28) Liberton, M.; Page, L. E.; O’Dell, W. B.; O’Neill, H.; Mamontov, E.; Urban, V. S.; Pakrasi,  
527 H. B. Organization and Flexibility of Cyanobacterial Thylakoid Membranes Examined by  
528 Neutron Scattering. *J. Biol. Chem.* **2013**, *288* (5), 3632–3640.  
529 <https://doi.org/10.1074/jbc.M112.416933>.
- 530 (29) Sarma, T. A. *Handbook of Cyanobacteria*, 0 ed.; CRC Press, 2012.  
531 <https://doi.org/10.1201/b14316>.
- 532 (30) Stanier, R. Y.; Deruelles, J.; Rippka, R.; Herdman, M.; Waterbury, J. B. Generic  
533 Assignments, Strain Histories and Properties of Pure Cultures of Cyanobacteria. *Journal of*  
534 *General Microbiology* **1979**, *111* (1), 1–61. <https://doi.org/10.1099/00221287-111-1-1>.
- 535 (31) Jaishankar, J.; Srivastava, P. Molecular Basis of Stationary Phase Survival and  
536 Applications. *Front. Microbiol.* **2017**, *8*, 2000. <https://doi.org/10.3389/fmicb.2017.02000>.
- 537 (32) Muthusamy, S.; Lundin, D.; Branca, R. M. M.; Baltar, F.; González, J. M.; Lehtiö, J.;  
538 Pinhassi, J. Comparative Proteomics Reveals Signature Metabolisms of Exponentially  
539 Growing and Stationary Phase Marine Bacteria. *Environmental Microbiology* **2017**, *19* (6),  
540 2301–2319. <https://doi.org/10.1111/1462-2920.13725>.
- 541 (33) Lavoie, M.; Le Faucheur, S.; Fortin, C.; Campbell, P. G. C. Cadmium Detoxification  
542 Strategies in Two Phytoplankton Species: Metal Binding by Newly Synthesized Thiolated  
543 Peptides and Metal Sequestration in Granules. *Aquatic Toxicology* **2009**, *92* (2), 65–75.  
544 <https://doi.org/10.1016/j.aquatox.2008.12.007>.
- 545 (34) Bridou, R.; Monperrus, M.; Gonzalez, P. R.; Guyoneaud, R.; Amouroux, D. Simultaneous  
546 Determination of Mercury Methylation and Demethylation Capacities of Various Sulfate-  
547 Reducing Bacteria Using Species-Specific Isotopic Tracers. *Environmental Toxicology and*  
548 *Chemistry* **2011**, *30* (2), 337–344. <https://doi.org/10.1002/etc.395>.

- 549 (35) Schuurmans, R. M.; Matthijs, J. C. P.; Hellingwerf, K. J. Transition from Exponential to  
550 Linear Photoautotrophic Growth Changes the Physiology of *Synechocystis* Sp. PCC 6803.  
551 *Photosynth Res* **2017**, *132* (1), 69–82. <https://doi.org/10.1007/s11120-016-0329-8>.
- 552 (36) Wu, Y.; Wang, W.-X. Thiol Compounds Induction Kinetics in Marine Phytoplankton  
553 during and after Mercury Exposure. *Journal of Hazardous Materials* **2012**, *217–218*, 271–  
554 278. <https://doi.org/10.1016/j.jhazmat.2012.03.024>.
- 555 (37) Morelli, E.; Ferrara, R.; Bellini, B.; Dini, F.; Di Giuseppe, G.; Fantozzi, L. Changes in the  
556 Non-Protein Thiol Pool and Production of Dissolved Gaseous Mercury in the Marine  
557 Diatom *Thalassiosira weissflogii* under Mercury Exposure. *Science of The Total*  
558 *Environment* **2009**, *408* (2), 286–293. <https://doi.org/10.1016/j.scitotenv.2009.09.047>.
- 559 (38) Wu, Y.; Wang, W.-X. Accumulation, Subcellular Distribution and Toxicity of Inorganic  
560 Mercury and Methylmercury in Marine Phytoplankton. *Environmental Pollution* **2011**, *159*  
561 (10), 3097–3105. <https://doi.org/10.1016/j.envpol.2011.04.012>.
- 562 (39) Bravo, A. G.; Le Faucheur, S.; Monperrus, M.; Amouroux, D.; Slaveykova, V. I. Species-  
563 Specific Isotope Tracers to Study the Accumulation and Biotransformation of Mixtures of  
564 Inorganic and Methyl Mercury by the Microalga *Chlamydomonas Reinhardtii*.  
565 *Environmental Pollution* **2014**, *192*, 212–215.  
566 <https://doi.org/10.1016/j.envpol.2014.05.013>.
- 567 (40) Wu, Y.; Wang, W.-X. Intracellular Speciation and Transformation of Inorganic Mercury in  
568 Marine Phytoplankton. *Aquatic Toxicology* **2014**, *148*, 122–129.  
569 <https://doi.org/10.1016/j.aquatox.2014.01.005>.
- 570 (41) Pickhardt, P. C.; Fisher, N. S. Accumulation of Inorganic and Methylmercury by Freshwater  
571 Phytoplankton in Two Contrasting Water Bodies. *Environ. Sci. Technol.* **2007**, *41* (1), 125–  
572 131. <https://doi.org/10.1021/es060966w>.
- 573 (42) Pickhardt, P. C.; Folt, C. L.; Chen, C. Y.; Klaue, B.; Blum, J. D. Impacts of Zooplankton  
574 Composition and Algal Enrichment on the Accumulation of Mercury in an Experimental  
575 Freshwater Food Web. *Science of The Total Environment* **2005**, *339* (1–3), 89–101.  
576 <https://doi.org/10.1016/j.scitotenv.2004.07.025>.
- 577 (43) Elbaz, A.; Wei, Y. Y.; Meng, Q.; Zheng, Q.; Yang, Z. M. Mercury-Induced Oxidative Stress  
578 and Impact on Antioxidant Enzymes in *Chlamydomonas Reinhardtii*. *Ecotoxicology* **2010**,  
579 *19* (7), 1285–1293. <https://doi.org/10.1007/s10646-010-0514-z>.
- 580 (44) Slaveykova, V. I.; Majumdar, S.; Regier, N.; Li, W.; Keller, A. A. Metabolomic Responses  
581 of Green Alga *Chlamydomonas Reinhardtii* Exposed to Sublethal Concentrations of  
582 Inorganic and Methylmercury. *Environ. Sci. Technol.* **2021**, *acs.est.0c08416*.  
583 <https://doi.org/10.1021/acs.est.0c08416>.
- 584 (45) Devars, S.; Avilés, C.; Cervantes, C.; Moreno-Sánchez, R. Mercury Uptake and Removal  
585 by *Euglena Gracilis*. *Archives of Microbiology* **2000**, *174* (3), 175–180.  
586 <https://doi.org/10.1007/s002030000193>.
- 587 (46) Narainsamy, K.; Farci, S.; Braun, E.; Junot, C.; Cassier-Chauvat, C.; Chauvat, F. Oxidative-  
588 Stress Detoxification and Signalling in Cyanobacteria: The Crucial Glutathione Synthesis  
589 Pathway Supports the Production of Ergothioneine and Ophthalmate: Ophthalmate an  
590 Evolutionary-Conserved Stress Marker. *Molecular Microbiology* **2016**, *100* (1), 15–24.  
591 <https://doi.org/10.1111/mmi.13296>.
- 592 (47) Narainsamy, K.; Marteyn, B.; Sakr, S.; Cassier-Chauvat, C.; Chauvat, F. Genomics of the  
593 Pleiotropic Glutathione System in Cyanobacteria. In *Advances in Botanical Research*;

- 594 Elsevier, 2013; Vol. 65, pp 157–188. [https://doi.org/10.1016/B978-0-12-394313-2.00005-](https://doi.org/10.1016/B978-0-12-394313-2.00005-6)  
595 6.
- 596 (48) Bellini, E.; Varotto, C.; Borsò, M.; Rugnini, L.; Bruno, L.; Sanità di Toppi, L. Eukaryotic  
597 and Prokaryotic Phytochelatin Synthases Differ Less in Functional Terms Than Previously  
598 Thought: A Comparative Analysis of *Marchantia Polymorpha* and *Geitlerinema* Sp. PCC  
599 7407. *Plants* **2020**, *9* (7), 914. <https://doi.org/10.3390/plants9070914>.
- 600 (49) Kelly, D. J. A.; Budd, K.; Lefebvre, D. D. The Biotransformation of Mercury in PH-Stat  
601 Cultures of Microfungi. *Canadian Journal of Botany* **2006**, *84* (2), 254–260.  
602 <https://doi.org/10.1139/b05-156>.
- 603 (50) Jones, G. J.; Palenik, B. P.; Morel, F. M. M. TRACE METAL REDUCTION BY  
604 PHYTOPLANKTON: THE ROLE OF PLASMALEMMA REDOX ENZYMES. *J Phycol*  
605 **1987**, *23* (s2), 237–244. <https://doi.org/10.1111/j.1529-8817.1987.tb04131.x>.
- 606 (51) Schaefer, J. K.; Morel, F. M. M. High Methylation Rates of Mercury Bound to Cysteine by  
607 *Geobacter Sulfurreducens*. *Nature Geoscience* **2009**, *2* (2), 123–126.  
608 <https://doi.org/10.1038/ngeo412>.
- 609 (52) Schaefer, J. K.; Rocks, S. S.; Zheng, W.; Liang, L.; Gu, B.; Morel, F. M. M. Active  
610 Transport, Substrate Specificity, and Methylation of Hg(II) in Anaerobic Bacteria.  
611 *Proceedings of the National Academy of Sciences of the United States of America* **2011**, *108*  
612 (21), 8714–8719. <https://doi.org/10.1073/pnas.1105781108>.
- 613 (53) Du, W.; Liu, Y.; Sun, J.; Wu, N.; Mai, Y.; Wang, C. The Aquatic Microbial Community: A  
614 Bibliometric Analysis of Global Research Trends (1991–2018). *fal* **2020**, *194* (1), 19–32.  
615 <https://doi.org/10.1127/fal/2020/1305>.
- 616 (54) Basińska, A. M.; Reczuga, M. K.; Gąbka, M.; Stróżecki, M.; Łuców, D.; Samson, M.;  
617 Urbaniak, M.; Leśny, J.; Chojnicki, B. H.; Gilbert, D.; Sobczyński, T.; Olejnik, J.;  
618 Silvennoinen, H.; Juszczak, R.; Lamentowicz, M. Experimental Warming and Precipitation  
619 Reduction Affect the Biomass of Microbial Communities in a Sphagnum Peatland.  
620 *Ecological Indicators* **2020**, *112*, 106059. <https://doi.org/10.1016/j.ecolind.2019.106059>.
- 621 (55) Lüring, M.; Eshetu, F.; Faassen, E. J.; Kosten, S.; Huszar, V. L. M. Comparison of  
622 Cyanobacterial and Green Algal Growth Rates at Different Temperatures: *Temperature and*  
623 *Phytoplankton Growth Rates*. *Freshwater Biology* **2013**, *58* (3), 552–559.  
624 <https://doi.org/10.1111/j.1365-2427.2012.02866.x>.
- 625 (56) Ji, M.; Liu, Z.; Sun, K.; Li, Z.; Fan, X.; Li, Q. Bacteriophages in Water Pollution Control:  
626 Advantages and Limitations. *Front. Environ. Sci. Eng.* **2021**, *15* (5), 84.  
627 <https://doi.org/10.1007/s11783-020-1378-y>.  
628